Local Causality in a Friedmann-Robertson-Walker Spacetime

Joy Christian*
Einstein Centre for Local-Realistic Physics, 15 Thackley End, Oxford OX2 6LB, United Kingdom

A local, deterministic, and realistic model within a Friedmann-Robertson-Walker spacetime with constant spatial curvature (S^3) is presented which describes simultaneous measurements of the spins of two fermions emerging in a singlet state from the decay of a spinless boson. Exact agreement with the probabilistic predictions of quantum theory is achieved in the model without data rejection, remote contextuality, superdeterminism, or backward causation. A singularity-free Clifford-algebraic representation of S^3 with vanishing spatial curvature and non-vanishing torsion is then employed to transform the model in a more elegant form. Several event-by-event numerical simulations of the model are presented, which confirm our analytical results with the accuracy of 4 parts in 10^4 parts.

arXiv:1405.2355v3 [quant-ph] 30 Apr 2016

Unlike our most fundamental theories of space and time, quantum theory happens to be incompatible with local causality [1]. This fact was famously recognized in 1935 by Einstein, Podolsky, and Rosen (EPR) [2]. They hoped, however, that perhaps quantum mechanics can be completed into a locally causal theory by addition of supplementary or hidden parameters. Today such hopes of maintaining both locality and realism within physics seem to have been undermined by Bell's theorem [1], with considerable support from experiments [3]. Bell set out to prove that no physical theory which is realistic as well as local in a sense espoused by Einstein can reproduce all of the statistical predictions of quantum mechanics [1]. The purpose of this paper is to show that it is, in fact, possible to reproduce the statistical predictions of quantum states such as the EPR-Bohm state in a locally causal manner, in the familiar Friedmann-Robertson-Walker spacetime (albeit viewed as a *non*-cosmological, terrestrial solution of Einstein's field equations).

A locally causal description of the measurement of the spins of two spacelike separated spin-$\frac{1}{2}$ particles which were products of the decay of a single spin-zero particle has been considered by Bell [1]. Based on Bohm's version of the EPR thought experiment, he considered a pair of spin-$\frac{1}{2}$ particles, moving freely after the decay in opposite directions, with particles 1 and 2 subject (respectively) to spin measurements along independently chosen unit directions $\mathbf{a}$ and $\mathbf{b}$, which may be located at a spacelike distance from one another. If initially the emerging pair has vanishing total spin, then its quantum mechanical spin state can be described by the entangled singlet state,

$$|\Psi_{\mathbf{n}}\rangle = \frac{1}{\sqrt{2}}\Big\{|\mathbf{n},\,+\rangle_1\otimes|\mathbf{n},\,-\rangle_2\,-\,|\mathbf{n},\,-\rangle_1\otimes|\mathbf{n},\,+\rangle_2\Big\}, \tag{1}$$

with $\mathbf{n}$ as arbitrary direction and $\boldsymbol{\sigma}\cdot\mathbf{n}\,|\mathbf{n},\,\pm\rangle = \pm\,|\mathbf{n},\,\pm\rangle$ describing the quantum mechanical eigenstates in which the particles have spin up or down in the units of $\hbar = 2$.

Our interest lies in an event-by-event reproduction of the probabilistic predictions of this entangled quantum state in a locally causal manner [1]. For any freely chosen measurement directions $\mathbf{a}$ and $\mathbf{b}$ in space there would be nine possible outcomes of the experiment in general, regardless of the distance between the directions. If we denote the angle between $\mathbf{a}$ and $\mathbf{b}$ by $\eta_{\mathbf{ab}}$ and the local measurement results 0, +1, or −1 about these directions by $\mathscr{A}$ and $\mathscr{B}$, then quantum mechanics is well known to predict the following joint probabilities for these results:

$$P_{12}^{+-}(\eta_{\mathbf{ab}}) = P\{\mathscr{A}=+1,\ \mathscr{B}=-1\mid\eta_{\mathbf{ab}}\} = \frac{1}{2}\cos^2\Big(\frac{\eta_{\mathbf{ab}}}{2}\Big), \tag{2}$$

$$P_{12}^{++}(\eta_{\mathbf{ab}}) = P\{\mathscr{A}=+1,\ \mathscr{B}=+1\mid\eta_{\mathbf{ab}}\} = \frac{1}{2}\sin^2\Big(\frac{\eta_{\mathbf{ab}}}{2}\Big), \tag{3}$$

$$P_{12}^{-+}(\eta_{\mathbf{ab}}) = P_{12}^{+-}(\eta_{\mathbf{ab}}), \tag{4}$$

$$P_{12}^{--}(\eta_{\mathbf{ab}}) = P_{12}^{++}(\eta_{\mathbf{ab}}), \tag{5}$$

$$P_{12}^{+0}(\eta_{\mathbf{ab}}) = P_{12}^{-0}(\eta_{\mathbf{ab}}) = P_{12}^{0+}(\eta_{\mathbf{ab}}) = P_{12}^{0-}(\eta_{\mathbf{ab}}) = 0, \tag{6}$$

and

$$P_{12}^{00}(\eta_{\mathbf{ab}}) = 0, \tag{7}$$

*Electronic address: jjc@alum.bu.edu

where the superscript 0 indicates no detection and the subscripts 1 and 2 label the particles [4]. The probability that the spin of the particle 1 will be detected parallel to $\mathbf{a}$ (regardless of whether particle 2 itself is detected) is also predicted by quantum mechanics. It is given by

$$P_1^+(\mathbf{a}) = P_1^-(\mathbf{a}) = \frac{1}{2}, \tag{8}$$

and likewise for particle 2 being detected parallel to $\mathbf{b}$. In what follows our goal is to demonstrate that, at least in the Friedmann-Robertson-Walker spacetime $\mathbb{R} \times \Sigma$ with a constant spatial curvature, the above probabilities can be reproduced within the original local model of Bell [1].

To this end, consider a spacelike hypersurface $\Sigma = S^3$ in a Friedmann-Robertson-Walker solution with $\kappa = +1$,

$$ds^2 = dt^2 - a^2(t)\, d\Sigma^2, \quad d\Sigma^2 = \left[\frac{d\rho^2}{1-\kappa\,\rho^2} + \rho^2 d\Omega^2\right], \tag{9}$$

where $\Sigma = S^3$ can be recovered by introducing $\chi = \sin^{-1}\rho$. Now, for $\kappa = +1$, the tangent bundle of S^3 happens to be trivial: $\mathrm{T}S^3 = S^3 \times \mathbb{R}^3$. This renders the tangent space at each point of S^3 to be isomorphic to $\mathbb{R}^3$. Thus local experiences of the experimenters within S^3 are no different from those of their counterparts within $\mathbb{R}^3$. The global topology of S^3, however, is dramatically different from that of $\mathbb{R}^3$ [5][6]. In particular, the triviality of $\mathrm{T}S^3$ means that S^3 is parallelizable [5]. Therefore, a global *anholonomic* frame can be specified on S^3 that fixes each of its points uniquely [5][6]. Such a frame renders S^3 diffeomorphic to the group SU(2) — *i.e.*, to the set of all unit quaternions:

$$S^3 \,=\, \left\{ \mathbf{H}(I\cdot\mathbf{v},\,\eta) \;\;\Big|\;\; ||\,\mathbf{H}(I\cdot\mathbf{v},\,\eta)\,|| \,=\, 1 \right\}. \tag{10}$$

Here we have parameterized each quaternion $\mathbf{H} \in S^3$ as

$$\mathbf{H}(I\cdot\mathbf{v},\,\eta) = \exp\{\,(I\cdot\mathbf{v})\,\eta\,\} \tag{11}$$

such that $I\cdot\mathbf{v}$, with a trivector I, is a bivector rotating about some vector $\mathbf{v} \in \mathbb{R}^3$, and η is half of the angle by which $\mathbf{H}$ stands rotated about $\mathbf{v}$. As in these definitions, in what follows we will be using the notation of geometric algebra [6][7][8]. Accordingly, all vector fields in $\mathbb{R}^3$ such as $\mathbf{v}$ and $\mathbf{w}$ will be assumed to satisfy the geometric product

$$\mathbf{v}\,\mathbf{w} \,=\, \mathbf{v}\cdot\mathbf{w} \,+\, \mathbf{v}\wedge\mathbf{w}, \tag{12}$$

with the duality relation $\mathbf{v}\wedge\mathbf{w} = I\cdot(\mathbf{v}\times\mathbf{w})$. In the next steps it will be useful to recall that $(\mathbf{v}\wedge\mathbf{w})^\dagger = -(\mathbf{v}\wedge\mathbf{w})$.

Consider now two unit quaternions from the closed set S^3, say $\mathbf{P}_o(\mathbf{n}\wedge\mathbf{e}_o,\,\eta_{\mathbf{ne}_o})$ and $\mathbf{Q}_o(\mathbf{z}\wedge\mathbf{s}_o,\,\eta_{\mathbf{zs}_o})$, defined as

$$\mathbf{P}_o \,=\, \cos(\,\eta_{\mathbf{ne}_o}) \,+\, \frac{\mathbf{n}\wedge\mathbf{e}_o}{||\mathbf{n}\wedge\mathbf{e}_o||}\,\sin(\,\eta_{\mathbf{ne}_o}) \tag{13}$$

and

$$\mathbf{Q}_o \,=\, \cos(\,\eta_{\mathbf{zs}_o}) \,+\, \frac{\mathbf{z}\wedge\mathbf{s}_o}{||\mathbf{z}\wedge\mathbf{s}_o||}\,\sin(\,\eta_{\mathbf{zs}_o}), \tag{14}$$

where $\mathbf{n} \in T_pS^3 \cong \mathbb{R}^3$ is an arbitrary unit vector in the tangent space T_pS^3 at some point p of S^3, $\mathbf{z}$ is a fixed reference vector in T_qS^3 at a different point q of S^3, and $\mathbf{e}_o$ and $\mathbf{s}_o$ are two other tangential vectors in T_qS^3. Here the bivector $I\cdot\mathbf{e}_o$ may be thought of as representing an individual spin within the pair of decaying particles in the singlet state, and the bivector $I\cdot\mathbf{s}_o$ may be thought of as representing the spin of the composite pair [4]. Note that, although $\mathbf{P}_o$ and $\mathbf{Q}_o$ are normalized to unity, their sum $\mathbf{P}_o + \mathbf{Q}_o$ need not be. In fact, they satisfy the following triangle inequality for arbitrary pairs of such quaternions,

$$||\mathbf{P}_o + \mathbf{Q}_o|| \,\leqslant\, ||\mathbf{P}_o|| \,+\, ||\mathbf{Q}_o||\,, \tag{15}$$

reflecting the metrical structure of S^3. Moreover, since S^3 is closed under multiplication, we also have $||\mathbf{P}_o\mathbf{Q}_o|| = 1$.

These constraints lead us to the following choice for the set of initial (or *complete*[1]) states $(\mathbf{P}_o,\,\mathbf{Q}_o)$ of our physical system:

$$\Lambda = \left\{ (\mathbf{P}_o,\,\mathbf{Q}_o) \;\;\Big|\;\; ||\mathbf{P}_o + \mathbf{Q}_o|| \,=\, \mathcal{N}(\,\eta_{\mathbf{ne}_o},\,\eta_{\mathbf{zs}_o}) \;\;\forall\,\mathbf{n} \right\}, \tag{16}$$

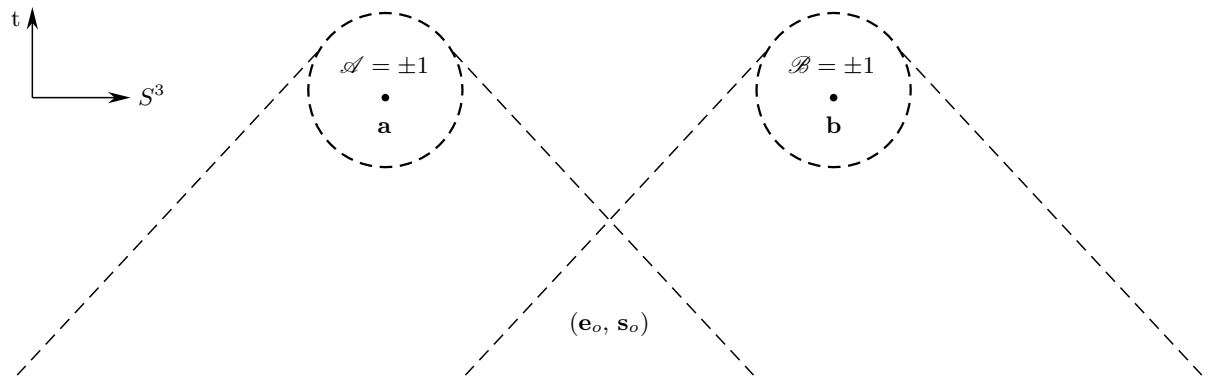

FIG. 1: The local results $\mathscr{A}(\mathbf{a};\, \mathbf{e}_o,\, \mathbf{s}_o)$ and $\mathscr{B}(\mathbf{b};\, \mathbf{e}_o,\, \mathbf{s}_o)$ are deterministically brought about by the common cause $(\mathbf{e}_o,\, \mathbf{s}_o)$.

where the value $\mathcal{N}$ of the norm is given by the variable

$$\mathcal{N}(\,\eta_{\mathbf{ne}_o},\ \eta_{\mathbf{zs}_o}) = 1 + \sin^2(\eta_{\mathbf{ne}_o}) + \left[-1 + \frac{2}{\sqrt{1 + 3\left(\frac{\eta_{\mathbf{zs}_o}}{\kappa\pi}\right)}}\right]^2, \tag{17}$$

which is necessarily a function of the angles $\eta_{\mathbf{ne}_o}$ and $\eta_{\mathbf{zs}_o}$. Note that we have allowed all three possible curvatures of Σ, with $\kappa = -1$ being equivalent to $\eta_{\mathbf{zs}_o} \to 2\pi - \eta_{\mathbf{zs}_o}$. The significance of this form of $\mathcal{N}$ will become clear soon.

If we now substitute expression (17) into the inequality

$$||\mathbf{P}_o||^2 \geqslant ||\mathbf{P}_o + \mathbf{Q}_o|| - 1\,, \tag{18}$$

which follows from multiplying the inequality (15) with $||\mathbf{P}_o|| = 1$ on both sides and simplifying, then [upon using

$$||\mathbf{P}_o||^2 = \cos^2(\,\eta_{\mathbf{ne}_o}) + \sin^2(\,\eta_{\mathbf{ne}_o}) \tag{19}$$

from Eq. (13)] the triangle inequality (15) simplifies to

$$|\cos(\,\eta_{\mathbf{ne}_o})| \geqslant -1 + \frac{2}{\sqrt{1 + 3\left(\frac{\eta_{\mathbf{zs}_o}}{\kappa\pi}\right)}}. \tag{20}$$

In what follows it is very important to recognize that this constraint is simply an expression of the intrinsic metrical and topological structures of S^3, and as such it holds for *all* vectors $\mathbf{n}$ for a given pair of initial states $(\mathbf{e}_o,\, \mathbf{s}_o)$; and, conversely, for *all* pairs of initial states $(\mathbf{e}_o,\, \mathbf{s}_o)$ for a given choice of vector $\mathbf{n}$. This can be easily verified by starting, for example, with a different pair of quaternions, say with the pair $\mathbf{P}'_o(\mathbf{n}' \wedge \mathbf{e}_o,\, \eta_{\mathbf{n}'\mathbf{e}_o})$ and $\mathbf{Q}_o(\mathbf{z} \wedge \mathbf{s}_o,\, \eta_{\mathbf{zs}_o})$, where

$$\mathbf{P}'_o = \cos(\,\eta_{\mathbf{n}'\mathbf{e}_o}) + \frac{\mathbf{n}' \wedge \mathbf{e}_o}{||\mathbf{n}' \wedge \mathbf{e}_o||} \sin(\,\eta_{\mathbf{n}'\mathbf{e}_o}), \tag{21}$$

and arriving at a similar constraint as the one in Eq. (20):

$$|\cos(\,\eta_{\mathbf{n}'\mathbf{e}_o})| \geqslant -1 + \frac{2}{\sqrt{1 + 3\left(\frac{\eta_{\mathbf{zs}_o}}{\kappa\pi}\right)}}. \tag{22}$$

This procedure can then be repeated for *all* vectors $\mathbf{n}'$, and—for a given vector $\mathbf{n}$—for *all* pairs of states $(\mathbf{e}'_o,\, \mathbf{s}'_o)$.

If we now let $\mathbf{e}_o \in T_qS^3$ and $\mathbf{s}_o \in T_qS^3$ be two random vectors, uniformly distributed over S^2, and let $\eta_{\mathbf{zs}_o}$ be a random scalar, uniformly distributed over $[0,\, \pi]$, then we can simplify the set (16) of complete or initial states as

$$\Lambda = \left\{(\mathbf{P}_o,\, \mathbf{Q}_o) \;\middle|\; |\cos(\,\eta_{\mathbf{ne}_o})| \geqslant -1 + \frac{2}{\sqrt{1 + 3\left(\frac{\eta_{\mathbf{zs_o}}}{\kappa\pi}\right)}}\ \forall\, \mathbf{n}\right\}. \tag{23}$$

By the previous results this set is invariant under the rotations of $\mathbf{n}$. Consequently, we identify $\mathbf{n}$ as a detector direction, and define the measurement events observed by (say) Alice and Bob—along their *freely chosen* detector directions $\mathbf{n} = \mathbf{a}$ and $\mathbf{n} = \mathbf{b}$—by two functions of the form

$$\pm\,1 \,=\, \mathscr{A}(\mathbf{a};\,\mathbf{e}_o,\,\mathbf{s}_o)\colon \mathbb{R}^3\times\Lambda \longrightarrow S^3 \cong \mathrm{SU}(2) \tag{24}$$

and

$$\pm\,1 \,=\, \mathscr{B}(\mathbf{b};\,\mathbf{e}_o,\,\mathbf{s}_o)\colon \mathbb{R}^3\times\Lambda \longrightarrow S^3 \cong \mathrm{SU}(2). \tag{25}$$

These functions are identical to those considered by Bell [1] apart from the choice of their codomain, which is now the compact space S^3 instead of a subset of $\mathbb{R}$. That such maps indeed exist can be seen easily by noting that $\mathbf{P}_o \to \pm 1$ as $\eta_{\mathbf{ne}_o} \to 0$ or π. More explicitly, we construct

$$S^3 \ni \pm 1 = \mathscr{A}(\mathbf{a};\,\mathbf{e}_o,\,\mathbf{s}_o) = -\,\mathrm{sign}\{\cos(\eta_{\mathbf{ae}_o})\} \text{ for a given } \mathbf{s}_o \tag{26}$$

and

$$S^3 \ni \pm 1 = \mathscr{B}(\mathbf{b};\,\mathbf{e}_o,\,\mathbf{s}_o) = +\,\mathrm{sign}\{\cos(\eta_{\mathbf{be}_o})\} \text{ for the same } \mathbf{s}_o. \tag{27}$$

Evidently, these functions define strictly local, realistic, and deterministically determined measurement events. Apart from the common cause $(\mathbf{e}_o,\,\mathbf{s}_o)$, which originates in the overlap of the backward lightcones of Alice and Bob as shown in Fig. 1, the event $\mathscr{A} = \pm 1$ depends *only* on the measurement direction $\mathbf{a}$ chosen freely by Alice; and analogously, apart from the common cause $(\mathbf{e}_o,\,\mathbf{s}_o)$, the event $\mathscr{B} = \pm 1$ depends *only* on the measurement direction $\mathbf{b}$ chosen freely by Bob. In particular, the function $\mathscr{A}(\mathbf{a};\,\mathbf{e}_o,\,\mathbf{s}_o)$ *does not* depend on either $\mathbf{b}$ or $\mathscr{B}$, and the function $\mathscr{B}(\mathbf{b};\,\mathbf{e}_o,\,\mathbf{s}_o)$ *does not* depend on either $\mathbf{a}$ or $\mathscr{A}$, just as demanded by Bell's formulation of local causality [1].

Now, to calculate the joint probabilities for observing the events $\mathscr{A} = \pm 1$ and $\mathscr{B} = \pm 1$ simultaneously along the directions $\mathbf{a}$ and $\mathbf{b}$, we follow the well known analysis carried out by Pearle for a formally similar local model [4]. Pearle begins by representing each pair of decaying particles by a point $\mathbf{r}$ in a state space made out of a ball of unit radius in $\mathbb{R}^3$. His state space is thus a well known representation of the group SO(3), each point of which corresponding to a rotation, with the direction $\mathbf{r}$ of length $0 \leqslant r \leqslant 1$ from the origin representing the axis of rotation and the angle πr representing the angle of rotation. The identity rotation corresponds to the point at the center of the ball. If we now identify the boundaries of two such unit balls, then we recover our 3-sphere, diffeomorphic to the double covering group of SO(3), namely SU(2). The pair of particles in this state space is represented by the quaternion $\mathbf{Q}_o$ defined in Eq. (14), which is rotating about the axis $\frac{\mathbf{z}\times\mathbf{s}_o}{||\,\mathbf{z}\times\mathbf{s}_o||}$ by the angle $2\eta_{\mathbf{zs}_o}$, with the unit vector $\mathbf{s_o}$ sweeping a 2-sphere within the 3-sphere [6][8].

The relationship between the rotation angle πr within Pearle's state space SO(3) and the rotation angle $2\eta_{\mathbf{zs}_o}$ within our state space $\mathrm{SU}(2) \cong S^3$ turns out to be simple:

$$\cos\Big(\frac{\pi}{2}r\Big) = \begin{cases} -1 + \dfrac{2}{\sqrt{1+3\left(\frac{\eta_{\mathbf{zs}_o}}{\kappa\pi}\right)}} \;=\; f(\eta_{\mathbf{zs}_o}), & (28) \\[2ex] -1 + \dfrac{2}{\sqrt{4-3\left(\frac{\eta_{\mathbf{zs}_o}}{\kappa\pi}\right)}} \;=\; f(\pi - \eta_{\mathbf{zs}_o}). & (29) \end{cases}$$

This can be recognized by first solving Eq. (28) for $\frac{\eta_{\mathbf{zs}_o}}{\kappa\pi}$ and then differentiating the solution with respect to r, which gives the probability density worked out by Pearle:

$$p(r) = \frac{1}{\kappa\pi}\frac{d\eta_{\mathbf{zs}_o}}{dr}(r) = \frac{4\pi}{3}\frac{\sin(\frac{\pi}{2}r)}{\left\{1+\cos\left(\frac{\pi}{2}r\right)\right\}^3}\,, \quad 0 \leqslant r \leqslant 1. \tag{30}$$

This function specifies the distribution of probability that a pair of particles is represented by the point $\mathbf{r}$ in the unit ball. Integrating this distribution from 0 to r we may also obtain the cumulative probability distribution in the ball:

$$C(r) \,=\, \int_0^r p(u)\,du \,=\, -\frac{1}{3} + \frac{4}{3\left\{1+\cos\left(\frac{\pi}{2}r\right)\right\}^2}\,. \tag{31}$$

This function specifies the probability of finding the pair in any state up to the state $\mathbf{r}$ within Pearle's state space. From solving Eq. (28) we see, however, that it is equal to our ratio $\frac{\eta_{\mathbf{zs}_o}}{\kappa\pi}$, and therefore also specifies the probability of finding the pair in any initial state up to the state $\mathbf{s}_o$.

For a given reference vector $\mathbf{z}$, the above relations allow us to translate between our representation in terms of the states $(\mathbf{e}_o,\, \mathbf{s}_o)$ in SU(2) and Pearle's representation in terms of the states $\mathbf{r}$ in SO(3). We can therefore rewrite our geometrical constraint (20) in terms of his state $\mathbf{r}$ as

$$|\cos(\eta_{\mathbf{a}\mathbf{e}_o})| \geqslant \cos\Big(\frac{\pi}{2}r\Big) \quad \text{and} \quad |\cos(\eta_{\mathbf{b}\mathbf{e}_o})| \geqslant \cos\Big(\frac{\pi}{2}r\Big), \tag{32}$$

where our vector $\mathbf{e}_o$ is related to his vector $\mathbf{r}$ as $\mathbf{e}_o = \mathbf{r}/r$. We are thus treating the axis $\mathbf{e}_o$ and the angle πr of the rotation of the spin as two independent random variables.

The equalities in the above inequalities correspond to the boundaries of the two circular caps on the spherical surface of radius r within the SO(3) ball considered by Pearle. The intersection of the two circular caps is then

$$\mathcal{I}(\pi r,\, \eta_{\mathbf{ab}}) = 4r^2\int_{\frac{\eta_{\mathbf{ab}}}{2}}^{\frac{\pi}{2}r} d\xi \sqrt{1 - \left\{\frac{\cos\left(\frac{\pi}{2}r\right)}{\cos(\xi)}\right\}^2} \quad \text{if } \eta_{\mathbf{ab}} \leqslant \pi r, \tag{33}$$

and zero otherwise. This area is derived by Pearle in the Appendix A of his paper. It is, however, not the correct overlap area for our model. What has been overlooked in Pearle's derivation are the contributions to $\mathcal{I}(\pi r,\, \eta_{\mathbf{ab}})$ from the *relative* rotations of the state $\mathbf{e}_o = \mathbf{r}/r$ along the directions $\mathbf{a}$ and $\mathbf{b}$. While the state $\mathbf{e}_o$ can be common to both $\mathbf{a}$ and $\mathbf{b}$, the corresponding rotations πr cannot be the same in general about both $\mathbf{a}$ and $\mathbf{b}$. An example of the difference can be readily seen from the relations (28) and (29), while heeding to the double covering in SU(2):

$$\pi\Delta r = \begin{cases} 2\,\cos^{-1}\left[-1 + \dfrac{2}{\sqrt{1 + \,3\left(\frac{\eta_{\mathbf{ab}}}{\pi}\right)}}\right] \;\text{ if }\; 0 \leqslant \eta_{\mathbf{ab}} \leqslant \frac{\pi}{2}, \\[2ex] 2\,\cos^{-1}\left[-1 + \dfrac{2}{\sqrt{4 - \,3\left(\frac{\eta_{\mathbf{ab}}}{\pi}\right)}}\right] \;\text{ if }\; \frac{\pi}{2} \leqslant \eta_{\mathbf{ab}} \leqslant \pi. \end{cases} \tag{34}$$

Evidently, $\Delta r = 0$ when $\eta_{\mathbf{ab}} = 0$ or π, and maximum when $\eta_{\mathbf{ab}} = \frac{\pi}{2}$. More generally, the effective radius of the spherical surface to which the circular caps belong must be "phase-shifted" to $r' = r\sqrt{\mathrm{h}(\eta_{\mathbf{ab}})}$ in our SU(2) model, where

$$\mathrm{h}(\eta_{\mathbf{ab}}) = \frac{3\pi}{8}\left\{\frac{\sin^2(\eta_{\mathbf{ab}})}{\pi\sin^2\left(\frac{1}{2}\eta_{\mathbf{ab}}\right) + \eta_{\mathbf{ab}}\cos(\eta_{\mathbf{ab}}) - \sin(\eta_{\mathbf{ab}})}\right\} \tag{35}$$

is the inverse of the function derived in Pearle's Eq. (23). The correct overlap area is then obtained by replacing r by r' in the differential area $dA = r^2 d\omega$ in Eq. (33) so that

$$\mathcal{I}(\pi r,\, \eta_{\mathbf{ab}}) \longrightarrow \mathcal{J}(\pi r,\, \eta_{\mathbf{ab}}) = \mathrm{h}(\eta_{\mathbf{ab}})\, \mathcal{I}(\pi r,\, \eta_{\mathbf{ab}}). \tag{36}$$

Using the probability density (30) and the overlap area (36), we can now calculate various joint probabilities as

$$\begin{aligned} P_{12}^{+-}(\eta_{\mathbf{ab}}) = P_{12}^{-+}(\eta_{\mathbf{ab}}) &= \int_{\frac{\eta_{\mathbf{ab}}}{\pi}}^{1} p(r)\, \frac{\mathcal{J}(\pi r,\, \eta_{\mathbf{ab}})}{4\pi r^2}\, dr \\ &= \frac{1}{2}\cos^2\Big(\frac{\eta_{\mathbf{ab}}}{2}\Big) \end{aligned} \tag{37}$$

and

$$\begin{aligned} P_{12}^{++}(\eta_{\mathbf{ab}}) = P_{12}^{--}(\eta_{\mathbf{ab}}) &= \int_{1-\frac{\eta_{\mathbf{ab}}}{\pi}}^{1} p(r)\, \frac{\mathcal{J}(\pi r,\, \pi - \eta_{\mathbf{ab}})}{4\pi r^2}\, dr \\ &= \frac{1}{2}\sin^2\Big(\frac{\eta_{\mathbf{ab}}}{2}\Big). \end{aligned} \tag{38}$$

These calculations of the joint probabilities are analogous to those by Pearle, except for using the area $\mathcal{J}(\pi r,\, \eta_{\mathbf{ab}})$.

Although the statistical effects of the constraints (32) in our model turn out to be almost identical to those in Pearle's model, the characteristics of the two models are markedly different. In our model the vectors $\mathbf{e}_o$ and $\mathbf{s}_o$ ensure in tandem that there are no initial states for which

$$|\cos(\eta_{\mathbf{ne}_o})| < \cos\Big(\frac{\pi}{2}r\Big) = -1 + \frac{2}{\sqrt{1+3\left(\frac{\eta_{\mathbf{zs}_o}}{\kappa\pi}\right)}}. \tag{39}$$

Consequently, the detectors of Alice and Bob can receive the spin states $\mathbf{e}_o$ only if the constraints (32) are satisfied. In other words, unlike Pearle's model, our model is not concerned about data rejection or detection loophole. In particular, in our model the fraction $\mathrm{g}(\eta_{\mathbf{ab}})$ of events in which both particles are detected is exactly equal to 1:

$$\mathrm{g}(\eta_{\mathbf{ab}}) = \frac{P_{12}^{+-}(\eta_{\mathbf{ab}})}{\frac{1}{2}\cos^2\left(\frac{\eta_{\mathbf{ab}}}{2}\right)} = \frac{P_{12}^{++}(\eta_{\mathbf{ab}})}{\frac{1}{2}\sin^2\left(\frac{\eta_{\mathbf{ab}}}{2}\right)} = 1 \ \ \forall\, \eta_{\mathbf{ab}} \in [0,\, \pi]. \tag{40}$$

Clearly, a measurement event cannot occur if there does not exist a state which can bring about that event. Since the initial state of the system is specified by the pair $(\mathbf{e}_o,\, \mathbf{s}_o)$ and not just by the vector $\mathbf{e}_o$, there are no states of the system for which $|\cos(\eta_{\mathbf{ne}_o})| < f(\eta_{\mathbf{zs}_o})$ for *any* vector $\mathbf{n}$. Thus a measurement event cannot occur for $|\cos(\eta_{\mathbf{ne}_o})| < f(\eta_{\mathbf{zs}_o})$, no matter what $\mathbf{n}$ is. As a result, there is a one-to-one correspondence between the initial state $(\mathbf{e}_o,\, \mathbf{s}_o)$ selected from the set (23) and the measurement events $\mathscr{A}$ and $\mathscr{B}$ specified by the Eqs. (26) and (27). This means, in particular, that the "fraction" $\mathrm{g}(\eta_{\mathbf{ab}})$ in our model is equal to 1 for all $\eta_{\mathbf{ab}}$, dictating the vanishing of the probabilities

$$P_{12}^{00}(\eta_{\mathbf{ab}}) = 1 + \mathrm{g}(\eta_{\mathbf{ab}}) - 2\,\mathrm{g}(0) = 0, \tag{41}$$

which follows from Pearle's Eq. (9). Moreover, from his Eq. (8) we also have $P_{12}^{+0}(\eta_{\mathbf{ab}}) = \frac{1}{2}\,[\,\mathrm{g}(0) - \mathrm{g}(\eta_{\mathbf{ab}})]$, giving

$$P_{12}^{+0}(\eta_{\mathbf{ab}}) = P_{12}^{-0}(\eta_{\mathbf{ab}}) = P_{12}^{0+}(\eta_{\mathbf{ab}}) = P_{12}^{0-}(\eta_{\mathbf{ab}}) = 0. \tag{42}$$

Together with the probabilities for individual detections,

$$P_1^{+}(\mathbf{a}) = P_1^{-}(\mathbf{a}) = P_2^{+}(\mathbf{b}) = P_2^{-}(\mathbf{b}) = \frac{1}{2}\,\mathrm{g}(0) = \frac{1}{2}\,, \tag{43}$$

the correlation between $\mathscr{A}$ and $\mathscr{B}$ then works out to be

$$\begin{aligned}\mathcal{E}(\mathbf{a},\, \mathbf{b}) \ &= \ \lim_{n\gg 1}\left[\frac{1}{n}\sum_{i\,=\,1}^{n}\mathscr{A}(\mathbf{a};\, \mathbf{e}_o^i,\, \mathbf{s}_o^i)\,\mathscr{B}(\mathbf{b};\, \mathbf{e}_o^i,\, \mathbf{s}_o^i)\right]\\ &= \ \frac{P_{12}^{++} \,+\, P_{12}^{--} \,-\, P_{12}^{+-} \,-\, P_{12}^{-+}}{P_{12}^{++} \,+\, P_{12}^{--} \,+\, P_{12}^{+-} \,+\, P_{12}^{-+}}\\ &= \ -\,\cos\left(\eta_{\mathbf{ab}}\right).\end{aligned} \tag{44}$$

Since all of the probabilities predicted by our local model in S^3 match exactly with the corresponding predictions of quantum mechanics, the violations of not only the CHSH inequality, but also Clauser-Horne inequality follow [3][8].

We have verified the above results in several event-by-event numerical simulations [9][10], which provide further insights into the strength of the correlation for different values of κ. As we discussed above, the rotation angle $\eta_{\mathbf{zs}_o}$ and the cumulative distribution function $C(r)$ are related by κ as

$$\frac{\eta_{\mathbf{zs}_o}}{\pi} = \kappa\, C(r), \tag{45}$$

where $|\kappa| \leqslant \infty$ can be interpreted as a *strength constant*. It is easy to verify in the simulations [9][10] that EPR-Bohm correlation results for $\kappa = +1$, whereas linear correlation results for $\kappa = 0$. The unphysical, or PR box correlation can also be generated in the simulation by letting $\kappa > +1$. On the other hand, setting $\kappa = -1$ [which is equivalent to letting $\eta_{\mathbf{zs}_o} \to 2\pi - \eta_{\mathbf{zs}_o}$ in Eq. (20)] leads back to the linear correlation [9][10]. The crucial observation here is that the strong, or quantum correlations are manifested only for $\kappa = +1$. Consequently, they can be best understood as resulting from the geometrical and topological structures of the quaternionic S^3, as defined, for example, in Eq. (10).

This conclusion can be further substantiated by first reflecting on a non-quaternionic or vector representation of the 3-sphere to model rotations, and then returning back to the quaternionic representation to appreciate the difference. It is well known that tensors such as ordinary vectors are not capable of modelling rotations in the physical space,

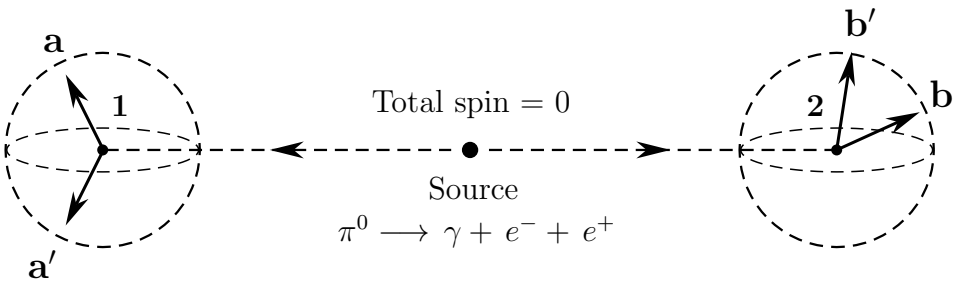

FIG. 2: A spin-less neutral pion decays into an electron-positron pair. Measurements of spin components on each separated fermion are performed at remote stations **1** and **2**, providing binary outcomes (respectively) along arbitrary directions **a** and **b**.

let alone modelling spinors in a singularity-free manner [6][8]. However, in the present context we are not interested in modelling all possible rotations and their all possible compositions in the physical space. We are only interested in establishing the correct correlation between some very special limiting points of the 3-sphere, namely between its scalar points such as $\mathscr{A}(\mathbf{a},\,\lambda) = \pm 1$ and $\mathscr{B}(\mathbf{b},\,\lambda) = \pm 1$, with λ being the "hidden variable" in the sense of Bell [1][6][8]. It turns out that in that case we can indeed model rotations (or more precisely, their spin values) by means of ordinary vectors and their inner products, but not with a single Riemannian metric [10]. A one-parameter family of *effective* metrics is required to model the relative spin values correctly. Given two vectors **u** and **v**, their inner product $g(\mathbf{u},\,\mathbf{v},\,\eta)$ is defined by the constraint $|\cos(\mathbf{u},\,\mathbf{v})| \geqslant f(\eta) \in [0,\,1]$, with the two extreme cases, namely $|\cos(\mathbf{u},\,\mathbf{v})| \geqslant 0$ and $|\cos(\mathbf{u},\,\mathbf{v})| \geqslant 1$, quantifying the weakest and the strongest topologies, respectively. Here the weakest topology dictated by $|\cos(\mathbf{u},\,\mathbf{v})| \geqslant 0$ is the topology of $\mathbb{R}^3$, where relatively few vectors **u** and **v** are orthogonal to each other. The strongest topology dictated by $|\cos(\mathbf{u},\,\mathbf{v})| \geqslant 1$, on the other hand, is more interesting, since in that case nearly *all* of the vectors **u** and **v** are orthogonal to each other. All intermediate topologies are dictated by *the effective metric*

$$g(\mathbf{u},\,\mathbf{v},\,\eta) = \begin{cases} \mathbf{u}\cdot\mathbf{v} & \text{if } \ |\mathbf{u}\cdot\mathbf{v}| \geqslant f(\eta) \\ 0 & \text{if } \ |\mathbf{u}\cdot\mathbf{v}| < f(\eta), \end{cases} \tag{46}$$

where (47)

$$f(\eta) \,:=\, -1 \,+\, \frac{2}{\sqrt{1+3\left(\frac{\eta}{\pi}\right)}} \quad \text{with } \ \eta \,\in\, [0,\,\pi]\,, \ \text{ and } \ \ \mathbf{u}\cdot\mathbf{v} := \cos(\mathbf{u},\,\mathbf{v}). \tag{48}$$

Evidently, the orthogonality of the vectors **u** and **v** is defined here by the condition $g(\mathbf{u},\,\mathbf{v},\,\eta) = 0$, depending on the parameter $\eta \,\in\, [0,\,\pi]$. It is this one-parameter family of metrics that has been implemented in the simulations [9][10]. The slight change in the notation of the distribution function from that in Eq. (20) is only for the coding convenience.

Returning to the singularity-free representation of S^3 specified in Eqs. (10) to (14), it is worth recalling that angular momenta are best described, not by ordinary polar vectors, but by pseudo-vectors, or bivectors, that change sign upon reflection [6]. One only has to compare a spinning object, like a barber's pole, with its image in a mirror to appreciate this elementary fact. The mirror image of a polar vector representing the spinning object is not the polar vector that represents the mirror image of the spinning object. In fact it is the negative of the polar vector that does the job. Therefore the spin angular momenta considered previously are better represented by a set of unit bivectors using the powerful language of geometric algebra [7]. They can be expressed in terms of graded bivector bases with sub-algebra

$$L_\mu(\lambda)\, L_\nu(\lambda) \,=\, -\,\delta_{\mu\nu} \,-\, \sum_\rho \,\epsilon_{\mu\nu\rho}\, L_\rho(\lambda)\,, \tag{49}$$

which span a tangent space at each point of S^3, with a choice of orientation $\lambda = \pm\,1$ [6]. Contracting this equation on both sides with the components a^μ and b^ν of arbitrary unit vectors **a** and **b** then gives the convenient bivector identity

$$\mathbf{L}(\mathbf{a},\,\lambda)\,\mathbf{L}(\mathbf{b},\,\lambda) \,=\, -\,\mathbf{a}\cdot\mathbf{b} \,-\, \mathbf{L}(\mathbf{a}\times\mathbf{b},\,\lambda)\,, \tag{50}$$

which is simply a geometric product between the unit bivectors representing the spin momenta considered previously:

$$\mathbf{L}(\mathbf{a},\,\lambda) \,=\, \lambda\, I\, \mathbf{a} \,=\, \lambda\, I\cdot\mathbf{a} \,\equiv\, \lambda(\mathbf{e}_x\wedge\mathbf{e}_y\wedge\mathbf{e}_z)\cdot\mathbf{a} \,=\, \pm 1 \text{ spin about the direction } \mathbf{a} \tag{51}$$

$$\text{and}\quad \mathbf{L}(\mathbf{b},\,\lambda) \,=\, \lambda\, I\, \mathbf{b} \,=\, \lambda\, I\cdot\mathbf{b} \,\equiv\, \lambda(\mathbf{e}_x\wedge\mathbf{e}_y\wedge\mathbf{e}_z)\cdot\mathbf{b} \,=\, \pm 1 \text{ spin about the direction } \mathbf{b}\,, \tag{52}$$

where the trivector $I := \mathbf{e}_x\wedge\mathbf{e}_y\wedge\mathbf{e}_z$ with $I^2 = -1$ represents the volume form on S^3 and ensures that $\mathbf{L}^2(\mathbf{n},\,\lambda) = -1$.

We are now in a position to derive the singlet correlation once again in a succinct and elegant manner. To this end, let the spin bivectors $\mp\,\mathbf{L}(\mathbf{s},\,\lambda^k)$ emerging from a source be detected by the detector bivectors $\mathbf{D}(\mathbf{a})$ and $\mathbf{D}(\mathbf{b})$, giving

$$S^3 \ni \mathscr{A}(\mathbf{a},\,\lambda^k) \,:=\, \lim_{\mathbf{s}_1\,\to\,\mathbf{a}} \big\{-\,\mathbf{D}(\mathbf{a})\,\mathbf{L}(\mathbf{s}_1,\,\lambda^k)\big\} \,=\, \left\{\begin{matrix} +1 & \text{if} \quad \lambda^k \,=\, +1 \\ -1 & \text{if} \quad \lambda^k \,=\, -1 \end{matrix}\right\} \text{ with } \Big\langle\, \mathscr{A}(\mathbf{a},\,\lambda^k)\,\Big\rangle \,=\, 0 \tag{53}$$

$$\text{and}\quad S^3 \ni \mathscr{B}(\mathbf{b},\,\lambda^k) \,:=\, \lim_{\mathbf{s}_2\,\to\,\mathbf{b}} \big\{+\,\mathbf{L}(\mathbf{s}_2,\,\lambda^k)\,\mathbf{D}(\mathbf{b})\big\} \,=\, \left\{\begin{matrix} -1 & \text{if} \quad \lambda^k \,=\, +1 \\ +1 & \text{if} \quad \lambda^k \,=\, -1 \end{matrix}\right\} \text{ with } \Big\langle\, \mathscr{B}(\mathbf{b},\,\lambda^k)\,\Big\rangle \,=\, 0\,, \tag{54}$$

where we assume the orientation λ of S^3 to be a random variable with 50/50 chance of being $+1$ or -1 at the moment of the pair-creation, making the spinning bivector $\mathbf{L}(\mathbf{n},\,\lambda^k)$ a random variable *relative* to the detector bivector $\mathbf{D}(\mathbf{n})$:

$$\mathbf{L}(\mathbf{n},\,\lambda^k) \,=\, \lambda^k\,\mathbf{D}(\mathbf{n}) \;\Longleftrightarrow\; \mathbf{D}(\mathbf{n}) \,=\, \lambda^k\,\mathbf{L}(\mathbf{n},\,\lambda^k)\,. \tag{55}$$

Moreover, as demanded by the conservation of angular momentum, we require the total spin to respect the condition

$$-\,\mathbf{L}(\mathbf{s}_1,\,\lambda^k) \,+\, \mathbf{L}(\mathbf{s}_2,\,\lambda^k) \,=\, 0 \;\Longleftrightarrow\; \mathbf{L}(\mathbf{s}_1,\,\lambda^k) \,=\, \mathbf{L}(\mathbf{s}_2,\,\lambda^k) \;\Longleftrightarrow\; \mathbf{s}_1 = \mathbf{s}_2 \equiv \mathbf{s} \quad \text{[cf. Fig. 2]}. \tag{56}$$

Evidently, in the light of the product rule (50) for the unit bivectors, the above condition is equivalent to the condition

$$\mathbf{L}(\mathbf{s}_1,\,\lambda^k)\,\mathbf{L}(\mathbf{s}_2,\,\lambda^k) \,=\, \big\{\,\mathbf{L}(\mathbf{s},\,\lambda^k)\big\}^2 \,=\, \mathbf{L}^2(\mathbf{s},\,\lambda^k) \,=\, -1\,. \tag{57}$$

The expectation value of simultaneous outcomes $\mathscr{A}(\mathbf{a},\,\lambda^k) = \pm 1$ and $\mathscr{B}(\mathbf{b},\,\lambda^k) = \pm 1$ in S^3 then works out as follows:

$$\mathcal{E}(\mathbf{a},\,\mathbf{b}) \,=\, \lim_{n\,\to\,\infty}\left[\frac{1}{n}\sum_{k\,=\,1}^{n}\,\mathscr{A}(\mathbf{a},\,\lambda^k)\,\mathscr{B}(\mathbf{b},\,\lambda^k)\right] \tag{58}$$

$$\,=\, \lim_{n\,\to\,\infty}\left[\frac{1}{n}\sum_{k\,=\,1}^{n}\,\left[\lim_{\mathbf{s}_1\,\to\,\mathbf{a}}\big\{-\,\mathbf{D}(\mathbf{a})\,\mathbf{L}(\mathbf{s}_1,\,\lambda^k)\big\}\right]\left[\lim_{\mathbf{s}_2\,\to\,\mathbf{b}}\big\{+\,\mathbf{L}(\mathbf{s}_2,\,\lambda^k)\,\mathbf{D}(\mathbf{b})\big\}\right]\right] \tag{59}$$

$$\,=\, \lim_{n\,\to\,\infty}\left[\frac{1}{n}\sum_{k\,=\,1}^{n}\,\lim_{\substack{\mathbf{s}_1\,\to\,\mathbf{a}\\ \mathbf{s}_2\,\to\,\mathbf{b}}}\big\{-\,\mathbf{D}(\mathbf{a})\,\big\}\,\big\{\,\mathbf{L}(\mathbf{s}_1,\,\lambda^k)\,\mathbf{L}(\mathbf{s}_2,\,\lambda^k)\,\big\}\,\big\{+\,\mathbf{D}(\mathbf{b})\,\big\}\right] \tag{60}$$

$$\,=\, \lim_{n\,\to\,\infty}\left[\frac{1}{n}\sum_{k\,=\,1}^{n}\,\lim_{\substack{\mathbf{s}_1\,\to\,\mathbf{a}\\ \mathbf{s}_2\,\to\,\mathbf{b}}}\big\{-\,\lambda^k\,\mathbf{L}(\mathbf{a},\,\lambda^k)\big\}\,\{-1\}\,\big\{+\,\lambda^k\,\mathbf{L}(\mathbf{b},\,\lambda^k)\big\}\right] \tag{61}$$

$$\,=\, \lim_{n\,\to\,\infty}\left[\frac{1}{n}\sum_{k\,=\,1}^{n}\,\lim_{\substack{\mathbf{s}_1\,\to\,\mathbf{a}\\ \mathbf{s}_2\,\to\,\mathbf{b}}}\Big\{+\,\big(\lambda^k\big)^2\,\mathbf{L}(\mathbf{a},\,\lambda^k)\,\mathbf{L}(\mathbf{b},\,\lambda^k)\Big\}\right] \tag{62}$$

$$\,=\, \lim_{n\,\to\,\infty}\left[\frac{1}{n}\sum_{k\,=\,1}^{n}\,\mathbf{L}(\mathbf{a},\,\lambda^k)\,\mathbf{L}(\mathbf{b},\,\lambda^k)\right] \tag{63}$$

$$\,=\, -\,\mathbf{a}\cdot\mathbf{b} \,-\, \lim_{n\,\to\,\infty}\left[\frac{1}{n}\sum_{k\,=\,1}^{n}\,\mathbf{L}(\mathbf{a}\times\mathbf{b},\,\lambda^k)\right] \tag{64}$$

$$\,=\, -\,\mathbf{a}\cdot\mathbf{b} \,-\, \lim_{n\,\to\,\infty}\left[\frac{1}{n}\sum_{k\,=\,1}^{n}\,\lambda^k\right]\mathbf{D}(\mathbf{a}\times\mathbf{b}) \tag{65}$$

$$\,=\, -\,\mathbf{a}\cdot\mathbf{b} \,+\, 0\,. \tag{66}$$

Here Eq. (59) follows from Eq. (58) by substituting the functions $\mathscr{A}(\mathbf{a},\,\lambda^k)$ and $\mathscr{B}(\mathbf{b},\,\lambda^k)$ from the definitions (53) and (54); Eq. (60) follows from Eq. (59) by using the "product of limits equal to limits of product" rule [which can be

verified by recognizing that the same quaternion $-\mathbf{D}(\mathbf{a})\,\mathbf{L}(\mathbf{a},\,\lambda^k)\,\mathbf{L}(\mathbf{b},\,\lambda^k)\,\mathbf{D}(\mathbf{b})$ results from the limits in Eqs. (59) and (60)]; Eq. (61) follows from Eq. (60) by (i) using the relation (55) [thus setting all bivectors in the spin bases], (ii) the associativity of the geometric product, and (iii) the conservation of spin angular momentum specified in Eq. (57); Eq. (62) follows from Eq. (61) by recalling that scalars such as λ^k commute with the bivectors; Eq. (63) follows from Eq. (62) by using $\lambda^2 = +1$, and by removing the superfluous limit operations; Eq. (64) follows from Eq. (63) by using the geometric product or identity (50), together with the fact that there is no third spin about the orthogonal direction $\mathbf{a}\times\mathbf{b}$ once the two spins are already detected along the directions $\mathbf{a}$ and $\mathbf{b}$; Eq. (65) follows from Eq. (64) by using the relations (55) and summing over the counterfactual detections of the "third" spins about $\mathbf{a}\times\mathbf{b}$; and Eq. (66) follows from Eq. (65) because the scalar coefficient of the bivector $\mathbf{D}(\mathbf{a}\times\mathbf{b})$ vanishes in $n\rightarrow\infty$ limit, since λ^k is a fair coin.

Note that, apart from the initial state λ^k, the only other assumption used in this derivation is that of the conservation of spin angular momentum (57). These two assumptions are necessary and sufficient to dictate the singlet correlations:

$$\mathcal{E}(\mathbf{a},\,\mathbf{b}) \,=\, \lim_{n\,\rightarrow\,\infty}\left[\frac{1}{n}\sum_{k\,=\,1}^{n}\,\mathscr{A}(\mathbf{a},\,\lambda^k)\,\mathscr{B}(\mathbf{b},\,\lambda^k)\right] \,=\, -\,\mathbf{a}\cdot\mathbf{b}\,. \tag{67}$$

This demonstrates that EPR-Bohm correlations are correlations among the scalar points of a quaternionic 3-sphere. Given this result, it is not difficult to derive the corresponding upper bound on the expectation values within S^3 [6][8]:

$$|\,\mathcal{E}(\mathbf{a},\,\mathbf{b}) \,+\, \mathcal{E}(\mathbf{a},\,\mathbf{b}') \,+\, \mathcal{E}(\mathbf{a}',\,\mathbf{b}) \,-\, \mathcal{E}(\mathbf{a}',\,\mathbf{b}')\,| \,\leqslant\, 2\sqrt{2}\,. \tag{68}$$

We have verified both of the above results in several numerical simulations [10][11]. The simulations are instructive on their own right and can be used for testing the effects of topology changes when the parameter $\eta\in[0,\,\pi]$ is varied.

In this paper we have shown that it is possible to reproduce the statistical predictions of quantum mechanics in a locally causal manner, at least for the simplest entangled state such as the EPR-Bohm state. In particular, we have shown that such a locally causal description of the singlet state in the sense of Bell is possible at least within the spherical topology of a well known Friedmann-Robertson-Walker spacetime, viewed as a non-cosmological, terrestrial solution of Einstein's field equations. More specifically, we have presented a local, deterministic, and realistic model within such a Friedmann-Robertson-Walker spacetime which describes simultaneous measurements of the spins of two fermions emerging in a singlet state from the decay of a spinless boson. We have then shown that the predictions of this locally causal model agree exactly with those of quantum theory, without needing data rejection, remote contextuality, superdeterminism, or backward causation. A Clifford-algebraic representation of the 3-sphere with vanishing spatial curvature and non-vanishing torsion then allows us to transform our model in an elegant form. Several event-by-event numerical simulations of the model have confirmed our analytical results with accuracy of at least 4 parts in 10^4 parts.

Acknowledgments

I wish to thank Fred Diether, Michel Fodje, Chantal Roth, and Albert Jan Wonnink for discussions and computing.

[1] J. S. Bell, Physics **1**, 195 (1964).
[2] A. Einstein, B. Podolsky, and N. Rosen, Phys. Rev. **47**, 777 (1935).
[3] J. F. Clauser and A. Shimony, Rep. Prog. Phys. **41**, 1881 (1978); A. Aspect, P. Grangier, and G. Roger, Phys. Rev. Lett. **49**, 91 (1982); G. Weihs *et al.*, Phys. Rev. Lett. **81**, 5039 (1998); B. Hensen *et al.*, Nature **526**, 682 (2015); L. K. Shalm *et al.*, arXiv:1511.03189 (2015); M. Giustina *et al.*, arXiv:1511.03190 (2015).
[4] P. M. Pearle, Phys. Rev. D **2**, 1418 (1970).
[5] M. Nakahara, *Geometry, Topology and Physics* (Adam Hilger, IOP Publishing Ltd, Bristol and New York, 1990).
[6] J. Christian, Int. J. Theor. Phys. **54**, 2042 (2015); DOI:10.1007/s10773-014-2412-2; See also arXiv:1501.03393 (2015).
[7] C. Doran and A. Lasenby, *Geometric Algebra for Physicists* (Cambridge University Press, Cambridge, 2003).
[8] J. Christian, *Disproof of Bell's Theorem: Illuminating the Illusion of Entanglement*, Second Edition (Brwonwalker Press, Boca Raton, Florida, 2014); See also arXiv:1106.0748 (2011) and arXiv:1211.0784 (2012).
[9] J. Christian, *A numerical simulation of the S^3 model for the EPR-Bohm correlation*, `http://rpubs.com/jjc/13965` (2014).
[10] J. Christian, *A 3-dimensional simulation of the 3-sphere model for the EPR-Bohm correlation*, `http://rpubs.com/jjc/84238` (2015) [see also `http://rpubs.com/jjc/99993` and `http://rpubs.com/jjc/105450`].
[11] A-J. Wonnink, `http://challengingbell.blogspot.co.uk/2015/03/numerical-validation-of-vanishing-of_30.html`, & C. F. Diether III, `http://challengingbell.blogspot.co.uk/2015/05/further-numerical-validation-of-joy.html`; See also C. F. Diether III, `http://www.sciphysicsforums.com/spfbb1/viewtopic.php?f=6&t=200&p=5550#p5514`.